EPR-Detected Folding Kinetics of Externally Located Cysteine-Directed Spin-Labeled Mutants of Iso-1-cytochrome *c*†

Kim DeWeerd,‡ Vladimir Grigoryants,‡ Yuhua Sun,‡ Jacquelyn S. Fetrow,§ and Charles P. Scholes*,‡

Department of Chemistry and Center for Biophysics and Biochemistry, University at Albany, SUNY, Albany, New York 12222, and GeneFormatics, Inc., 5830 Oberlin Drive, Suite 200, San Diego, California 92121

Received July 9, 2001; Revised Manuscript Received October 8, 2001

ABSTRACT: We report the application of our newly developed dielectric resonator-based flow and stopped-flow kinetic EPR systematically to probe protein folding in yeast iso-1-cytochrome *c* at cysteine-directed spin-labeled locations. The locations studied have not been previously directly probed by other techniques, and we observe them on a time scale stretching from 50 μs to seconds. On the basis of crystal structure and homology information, the following mutation-tolerant, externally located cysteine labeling sites were chosen (in helices, T8C, E66C, and N92C; in loops, E21C, V28C, H39C, D50C, and K79C), and labeling at these sites was not destabilizing. Dilution of denaturant was used to induce folding and thereby to cause a change in the spin label EPR signal as folding altered the motion of the spin label. Under folding conditions, including the presence of imidazole to eliminate kinetic trapping due to heme misligation, a phase of folding on the 20−30 ms time scale was found. This phase occurred not only at the T8C and N92C labeling sites in the N- and C-terminal helices, where such a phase has been associated with folding in these helices, but overall at labeling sites throughout the protein. In the absence of imidazole the 20−30 ms phase disappeared, and another phase having the time scale of 1 s appeared throughout the protein. There was evidence under all conditions for a burst phase on a scale of less than several milliseconds which occurred at labeling positions V28C, H39C, D50C, E66C, and K79C in the middle of the protein sequence. At spin-labeled D50C rapid-mix flow EPR indicated a very short ∼50 μs phase possibly associated with the prefolding or compaction of the loop to which D50 belongs. Spin labels have been criticized as perturbing the phenomena which they measure, but our spin labeling strategy has reported common kinetic themes and not perturbed, disconnected kinetic events.

As a probe for protein structure and function, the nitroxide spin label was originally developed to measure change in local protein conformation (*1*). The spin label sensitively reports local mobility in the vicinity of its attachment site and impediment to that mobility from the surroundings. Theoretical (*2*) or empirical (*3*) line shape analysis provides information on the 0.1−100 ns time scale and on restriction of the motion. The utility of spin labeling was markedly improved by the pioneering work of Hubbell and co-workers, who combined site-directed cysteine mutagenesis and cysteine-specific spin labeling to attach site-directed spin labels in new locations throughout proteins (*4*−*7*). The position of cysteine mutation was notably scanned throughout T4 lysozyme (*8*, *9*), and characteristic line shape signatures from labels at surface helix sites, tertiary contact sites, buried sites, and loop sites were determined. Such studies provided a background of empirical evidence on the type of signal to be expected from attachment at a particular site. Crystal studies of T4 lysozyme derivatives separately spin labeled at external helical sites and at a point of tertiary contact have shown how the protein environment, both nearby and more distant, establishes hydrophobic interactions and hydrogen bonds with the spin label that stabilize the conformation of its disulfide linkage and nitroxide ring (*10*). The crystal structure has provided a link between the dynamics of the spin label side chain, reflected in the EPR[1] spectrum, and local protein structure (*10*). Cysteine-directed spin labeling has opened a valuable area for following, predicting, and characterizing the fold of a protein, but it has so far been done under equilibrium conditions.

† This work was partially supported by National Science Foundation Grant MCB-9817598 and NIH Grant GM-35103. Acknowledgment is made to the donors of the Petroleum Research Fund, administered by the American Chemical Society, for partial support of this research (ACS-PRF Grant 34132-AC4).

* Address correspondence to this author at the Department of Chemistry, University at Albany, SUNY, Albany, NY 12222. Tel: 518-442-4551. Fax: 518-442-3462. E-mail: cps14@albany.edu.

‡ Department of Chemistry and Center for Biochemistry and Biophysics, University at Albany.

§ GeneFormatics, Inc.

[1] Abbreviations: EPR, electron paramagnetic resonance; DR, dielectric resonator; CW, continuous wave (as opposed to transient); ns, nanosecond; μs, microsecond; ms, millisecond; mW, milliwatt; ν_e, EPR frequency; MTSSL, methanethiosulfonate spin label; GdnHCl, guanidinium hydrochloride (Sigma 99.5% ultrapure); CD, circular dichroism; UV−vis, ultraviolet−visible spectroscopy; T_m, thermal melting temperature; C_m, the GdnHCl concentration at the midpoint of the GdnHCl-induced unfolding transition as expressed in molarity; iso-1-cyt *c*, yeast iso-1-cytochrome *c*; SL, ending added to a variant of iso-1-cyt *c* to indicate cysteine labeling; C102-SL, iso-1-cyt *c* spin labeled at its naturally occurring Cys102; C102S, iso-1-cyt *c* with a Cys102 → Ser102 mutation made to remove the wild-type Cys102. Amino acid single letter abbreviations: C, cysteine; D, aspartic acid; E, glutamic acid; H, histidine; K, lysine; L, leucine; N, asparagine; T, threonine; V, valine.

10.1021/bi011414n CCC: $20.00
Published on Web 11/27/2001

Our goal has been to combine the power of site-directed spin labeling with rapid-mix flow and stopped-flow EPR to follow the time variation of probe immobilization and to characterize protein substructures as they kinetically fold. This has required major technological advances in EPR, notably of mini microwave resonators tightly integrated to low dead volume, low dead time mixing devices. These devices must have high EPR sensitivity but low sensitivity to flow and stopped-flow induced noise. The major initial advance was a mini dielectric resonator (30-fold higher EPR sensitivity than commercial metallized EPR cavities) connected to a grid mixer to provide a fluid-flow structure with ~5 μL dead volume and ~1.5 μL sample volume (*11*). The dead time was ~7 ms, and the initial application was to the folding of 100 μM spin-labeled iso-1-cytochrome *c* (*12*). Two orders of magnitude improvement in kinetic resolution was later achieved when the dielectric resonator was intimately integrated to a micro ball mixer with submicroliter dead volume and dead times in the 100 μs regime (*13*).

Our choice for study has been cytochrome *c* because it is a protein for which there is a large inventory of folding information, albeit generally not information on the particular sites and side chains where we attach labels. Its folding was initially followed from optical changes at the heme and from heme-induced tryptophan fluorescence quenching which reports overall compacting of the cytochrome structure (*14*−*16*). The refolding kinetics for yeast and horse heart cytochrome *c* have been deconvoluted into at least three exponential phases observable for times longer than a millisecond (*15*−*17*): a fast phase in the 5−100 ms range, an intermediate phase in the 0.5−1 s range, and a minor slow phase in the 5−25 s range. The fast 5−100 ms phase has been a major focus of deuterium−hydrogen exchange of amide protons, a technique developed by Englander and co-workers (*18*), and is thought to reflect the critical rate-determining step of cytochrome folding due to nucleation collapse associated with the N- and C-terminal helices (*18*−*21*). Native state deuterium−hydrogen exchange at various low concentrations of denaturant was extrapolated to predict a folding pathway whereby the N- and C-terminal helices (substructure I) folded first, the 60's helix and loop A (substructure II) folded second, loops B and C (substructure III) folded third, and loop D (substructure IV) folded last (*22*, *23*). (See Figure 1 and Table 1 for positions of the relevant helices and loops.) The intermediate 0.5−1 s phase was attributed to states trapped with improper heme−histidine ligation that will convert into properly folded protein following dissociation of the non-native histidine iron ligands. Recent work of Nall and co-workers (*24*, *25*) altered such misligation by mutating the relevant histidines, and folding methods which replaced histidine by excess imidazole or lowered the pH eliminate this misligation phase (*15*, *20*). The slowest phase is most likely due to cis/trans isomerization of prolyl peptide bonds (*26*). These foregoing kinetic phases were determined from rapid-mix and/or stopped-flow techniques with millisecond or longer dead times. There also were changes occurring within the dead time, too early explicitly to be measured. What was initially called a "burst" stage of folding (decay time ≤5 ms) was suggested to be formation of a compact state with incompletely defined helical structure (*17*, *27*, *28*). The explicit elucidation of very early submillisecond folding/compaction has been the subject of intense investigation; see ref *29*. For cytochrome *c* the burst has been sensed by tryptophan fluorescence quenching, which reports a rapidly diminished heme iron-to-Trp59 separation (*30*, *31*) and by heme-centered spectroscopies monitoring heme-centered ligation (*32*, *33*); folding/compaction may start as early as 50 μs after initiation of folding. Submillisecond small-angle X-ray scattering showed that cytochrome *c* collapses to a compact structure before folding to its final state (*34*). A fundamental question is whether early folding is simply a response of a polymer to change in solvent quality (*21*) or whether it represents an early folding event with a specific energy barrier and activation energy (*30*, *35*) that precedes the critical millisecond, rate-limiting step of cytochrome folding.

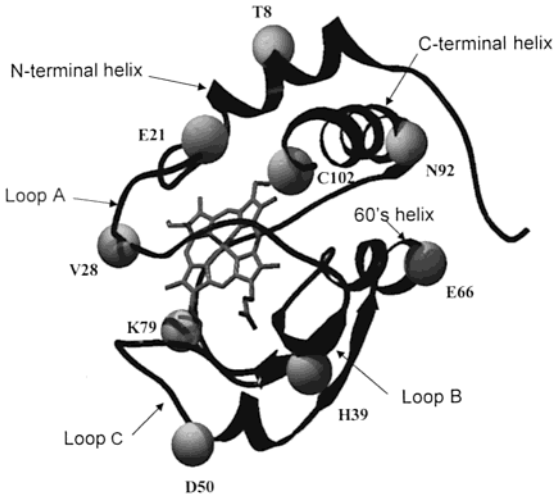

FIGURE 1: Ribbon diagram of yeast iso-1-cyt *c* showing loop and helical substructural regions and residues where cysteine mutations were made and where labeling was done. (Loop D happens to be in the back in this presentation.)

Table 1: Summary of Amino Acids That Have Been Mutated to Cysteine

residue[a]	labeled variant	secondary structure[b]	substructure[c]	substitutions[d]
Thr8	T8C-SL	N-helix	I	KTNRDS
Glu21	E21C-SL	loop A	II	EDQGNAK
Val28	V28C-SL	loop A	II	KTVIQAE
His39	H39C-SL	loop B	III	KQTHAV
Asp50	D50C-SL	loop C	III	TDEANK
Glu66	E66C-SL	60's helix	II	EADNGQKS
Lys79	K79C-SL	loop D	IV	TK
Asn92	N92C-SL	C-helix	I	ANQGEVKDTL

[a] Name and number of the residue to be replaced in the C102S protein, where the wild-type Cys102 is replaced by Ser. Numbering is based on alignment of other eukaryotic cytochromes *c* so that residues in yeast are numbered from −5 to +103. [b] The secondary structure in which the residue is found. [c] The partially unfolded substructure from native state H-exchange (*22*) in which the particular residue is found. The work of Bai et al. predicts that the order of folding should be I, II, III, IV. [d] These are the other amino acids found at this position in 106 eukaryotic cytochromes *c*.

Following the development of dielectric resonator-based stopped-flow EPR (*11*), we monitored the kinetics of protein folding as the folding altered the mobility of a cysteine-specific spin label, methanethiosulfonate spin label, MTSSL (*12*). The spin label for this initial study was attached at the sole cysteine (Cys102) occurring within the C-terminal helix of yeast iso-1-cyt *c*. Showing behavior which has generally

been true for our subsequent cysteine-directed spin labels, the spin label attached to unfolded protein demonstrated subnanosecond mobility and sharp, intense derivative EPR features, whereas the label on the folded protein was more encumbered by its environment and showed broader and less intense derivative EPR features indicating nanosecond or longer tumbling times. The spin label on the folded protein generally does retain some limited mobility with respect to the tumbling protein. (See, for example, Figure 2 of Qu et al. (*12*) or Figure 3A here.) Folding, observed following dilution of denaturant, was reported by the spin label at 2 °C as a 60−100 ms exponential process compatible with previously reported C-terminal helical formation (*18, 20*). At pH 6 the spin label sensed a slower misligation step occurring on the order of 1 s as well as a phase with 100 ms time. This work established the principle that dielectric resonator-based stopped-flow EPR could measure rapid kinetics of protein folding/helix formation reported by a spin label monitoring local motion in the vicinity of Cys102. Although this work (*12*) monitored the EPR signal at a single field, it was possible to monitor the entire EPR spectrum of the folding protein at various times after the start of folding by a combination of rapid magnetic field scanning and variable velocity flow EPR (*36*). In the course of work of Qu et al. (*12*) there was evidence of a faster probe immobilization and an incipient "burst" of folding that occurred in a time less than the ∼7 ms dead time of the original stopped-flow apparatus. To resolve such a faster refolding process, a micro ball mixer with submicroliter dead volume was integrated with the dielectric resonator (*13*). Then by monitoring the spin label signal at different flow velocities, the kinetics of probe immobilization of the Cys102-labeled iso-1-cyt *c* were followed to times as short as 100 μs following the start of folding. This work provided direct evidence for a burst of folding or protein compacting as monitored by the spin label at C102 that occurred within 150 μs of mixing at 20 °C and within 500 μs of mixing at 7 °C. There clearly was a temperature dependence to this burst, which may well imply a specific energy barrier and an activation energy to the early submillisecond folding process.

The position of a cysteine-bound label has provided EPR signals that vary with local structure and mobility under equilibrium conditions (*8*). Following our technical improvements to flow and stopped-flow EPR, we recognized that kinetic folding events could likewise be monitored in the vicinity of the labeling site, and then throughout a protein, if site-directed cysteine mutants could be made and mutant protein generated. The idea was that cysteine-specific spin labeling at different amino acid locations would probe for the formation of localized structures and would distinguish widespread global folding phenomena if probes throughout the protein happened to report a common time phase to their folding. It happened that wild-type Cys102 had deficiencies as a labeling site. Characterization carried out in Qu et al. (*12*) made us aware that labeling the Cys102 position had led to a 20 °C lower melting temperature than that of unlabeled wild-type protein. The location of the Cys102 sulfur prior to labeling is a region of hydrophobic packing (*37*), and so Cys102 labeling from within that region had destabilized the protein, probably by distorting the hydrophobic packing. Thus, a subsequent consideration in designing new labeling sites was to pick those sites which, when mutated to cysteine and spin labeled, were less perturbing to folding. In Table 1 we list the positions for labeling and indicate the diversity of substitutions that are tolerated at each labeling position from the inventory of 106 eukaryotic cytochromes *c* (*38*). In Figure 1 we show those positions within the iso-1-cyt *c* molecule where mutations were separately created for the present work. Those sites which were intended to be nonperturbing happened primarily to be at external, solvent-accessible positions, either in loop regions or in the hydrophilic external regions of helices. To obtain these sites and the subsequent protein in sufficient amount for stopped-flow and flow kinetic studies, a reliable method was developed for creating site-directed mutants of iso-1-cyt *c*. In contrast to our former yeast *Saccharomyces cerevisiae* expression system, large quantities of mutant protein were obtained using an *Escherichia coli* plasmid expression system originally developed by Mauk and coworkers (*39*) and then modified by Pielak (*40*) and Bowler (*41*) (personal communication). We now provide a detailed comparison, both between different labels and with preexisting findings from other technques, of kinetic folding behavior reported by the cysteine-directed spin labels at locations not previously probed. In addition, we present the expression system, the mutagenesis strategy, and the characterization of cysteine-directed mutants by CD and EPR spectroscopies.

EXPERIMENTAL PROCEDURES

Preparations

Materials for protein purification, spin labeling, protein denaturation, DNA purification, and DNA sequencing were obtained according to details found in the Supporting Information. Because of the comparatively low yield from growing mutant yeast iso-1-cyt *c* in yeast, an *E. coli* expression system, which contains both the yeast iso-1-cyt *c* gene and the heme lyase gene that attaches the heme to the cytochrome, was investigated (*39, 40*). The relevant plasmid was kindly provided by Professor Bruce Bowler, University of Denver, and this plasmid had the naturally occurring Cys102 of yeast iso-1-cyt *c* mutated to serine to prevent confusion when we were inserting and labeling other non-native mutant cysteines. C102S was the starting point for further cysteine mutation at locations indicated in Table 1 and Figure 1. The properties of C102S are extremely similar to those of native protein (*41, 42*), and *we routinely refer to C102S as "wild type"*. Site-directed mutagenesis aimed at creating new cysteine mutations of the CYC1 gene was performed using a PCR-based megaprimer procedure (*43*−*46*) given in the Supporting Information. Cultures of *E. coli* having a liquid volume of 10 L and harboring the mutated CYC1 gene were grown overnight in a Brunswick fermentor and purified according to previous methods (*47*−*49*) which are elaborated in the Supporting Information. Quantities (100 mg) of purified mutant protein were obtained from such an overnight fermentor growth. The purity of the protein was confirmed by SDS−PAGE (*49*) and by mass spectroscopic measurements. The general procedure for making MTSSL-labeled cysteine derivatives of iso-1-cyt *c* followed the procedure of Qu et al. (*12*). Spin-labeled variants are given the ending "SL".

Physical Methods

Mass Spectroscopy. Protein molecular weights were obtained from mass deconvoluted electrospray ionization spectra. Spectra were obtained on either a Finnigan TSQ 700 or a Finnigan LCQ DECA ion trap mass spectrometer (San Jose, CA) by infusion from a 49/49/2 water/acetonitrile/acetic acid solution.

UV−Vis Spectroscopy. Iso-1-cyt *c* concentrations were determined beforehand at room temperature by absorption spectroscopy at 410 nm on the Shimadzu Model CN 1601PC spectrophotometer using a heme extinction coefficient of 106.1×10^3 L M^{-1} cm^{-1} (*50*). Heme spectra of cysteine mutants were indistinguishable from those of wild type. The samples used were in the ferricytochrome state as determined from their visible 500−600 nm spectra (ref *38*, p 51).

CD Spectroscopic Characterization. CD data were collected from iso-1-cyt *c* at a concentration of 10 μM in 100 mM pH 5.0 sodium acetate buffer by use of an Aviv 62DS spectrometer fitted with a thermostated sample changer containing 0.1 cm quartz cuvettes. CD spectra that are an indicator of helical content were monitored in the far-UV from 200 to 250 nm. To characterize the thermal denaturation of mutant proteins with and without spin label, denaturation studies were carried out as in Qu et al. (*12*) by monitoring changes in ellipticity with respect to temperature at 222 nm. The purpose of these studies was to determine the melting temperature, T_m, at the midpoint of the thermal melting transition and the enthalpy of melting, ΔH_m. Far-UV CD measurements were also used to monitor the profile of GdnHCl-induced denaturation as a complement to EPR monitoring of denaturation.

Standard CW (Continuous Wave) EPR Spectroscopy. The EPR system was a Bruker ER-200 D-SRC X-band spectrometer which was interfaced to a Compaq 386 PC equipped with an IBM analog-to-digital converter and Scientific Software Services Systems (Bloomington, IL) EW 2.41A software for collecting both CW and transient data. Standard first derivative ($d\chi''/dH$) EPR spectroscopy was performed with a small, high-sensitivity dielectric resonator-based EPR probe (*11*). Power and modulation were chosen so as not to lead to broadening of the EPR spectrum. Spin-labeled samples had an approximate 1 μL volume contained within a 0.6 mm o.d., 0.8 mm i.d. quartz capillary (VitroCom Inc., Mountain Lakes, NJ).

Rapid-Mix Flow and Stopped-Flow EPR. Since obtaining and comparing kinetic data for times greater than a millisecond on our series of cysteine-directed mutants was our major focus, the rapid ball mixer system developed and calibrated by Grigoyrants et al. (*13*) was optimized for high sensitivity in the EPR stopped-flow mode. This stopped-flow EPR system was notably useful for weak signals of some mutant spin label systems where the difference between folded and unfolded signals was smaller than the difference seen from the originally studied C102-SL. Because of its relatively large volume and dead volume, this stopped-flow system provided a severalfold larger signal than that originally used for rapid-flow EPR (*13*). The present stopped-flow measurements used the ball mixer system with a larger EPR-active volume of 1.5 μL and a dead time of ~4 ms. This mixer device was intimately integrated to a dielectric resonator EPR probe, whose prototype is described in Sienkiewicz et al. (*11*) and which has been significantly modified by Grigoryants et al. (*13*). In stopped-flow mode the present system allowed us to achieve 60 shots per mL of reactant.

In contrast, a different ball mixer system developed specifically for flow EPR had a minimal EPR-active volume of ~0.36 μL and a minimal dead time when used with fastest flow rate of 65 μs. The flow system with such a ball mixer requires separate measurement of the signal intensity for each flow velocity. It was applied for this present work to elucidate the burst kinetics of D50C-SL, a mutant which exhibits a large, but very fast, burst phase.

Folding for flow and stopped-flow measurements was routinely induced by mixing GdnHCl-denatured protein in 1:1 fashion with folding buffer. The Update Instrument (Madison, WI) programmable ram driver was used to stop and start microliter volumes of fluid in the stopped-flow mode and to provide variable flow rates in the flow mode. Temperatures from 20 to 5 °C were maintained by coolant provided by a Neslab Model RTE-9B refrigerated circulating bath which was flowed about storage syringes, liquid delivery tubes, and the mixer body as the temperature was monitored by a thermocouple mounted on the resonator body.

RESULTS

Mass Spectroscopy. Mass spectroscopic measurements showed that the cysteine mutants differed from wild-type C102S only by the expected change of the relevant mutated amino acid. There was no deletion or insertion. For mutant yeast iso-1-cyt *c* expressed in *E. coli* the Lys72 was not trimethylated as it is in yeast. As shown in Table S-2 of the Supporting Information, all weights were within 5 AMU from the expected weight (out of ~12500 AMU), and the standard deviation from the expected weight was ±3 AMU.

CD Spectroscopic Characterization. The spin label modifications at all of the external labeling sites listed in Table 1 were not destabilizing, as has also been generally noted for cysteine-directed mutants of T4 lysozyme located on external loops and helices (*8*). The stability was indicated both by far-UV CD spectra which show characteristic helical signatures for all cysteine-labeled mutants similar to that of wild-type C102S (Supporting Information, Figure S-2) and by melting temperatures that were determined from CD-monitored thermal melting curves (Supporting Information, Table S-3 and Figure S-3). The melting temperatures, T_m, of the external mutants when labeled with MTSSL were equal to or slightly above the melting temperatures of their respective unlabeled counterparts and within several degrees of the melting temperature of C102S.

Chemical and thermal reversibility of unfolding was demonstrated for spin-labeled mutants. When denatured to 80 °C (at least 25 °C beyond the unfolding transition) for 20 min and then rapidly cooled to 5 °C to refold, all spin-labeled variants except K79C-SL and N92C-SL showed at least 80% recovery of their native CD helical signature, and K79C-SL and N92C-SL showed 50% recovery. All of the GdnHCl-unfolded cysteine-labeled mutant samples refolded to 100% of their native CD helical signature. At pH 5.0 and room temperature, where most of the kinetic measurements were made, the approximate midpoint of the GdnHCl unfolding transition was 1 M GdnHCl; greater than 90%

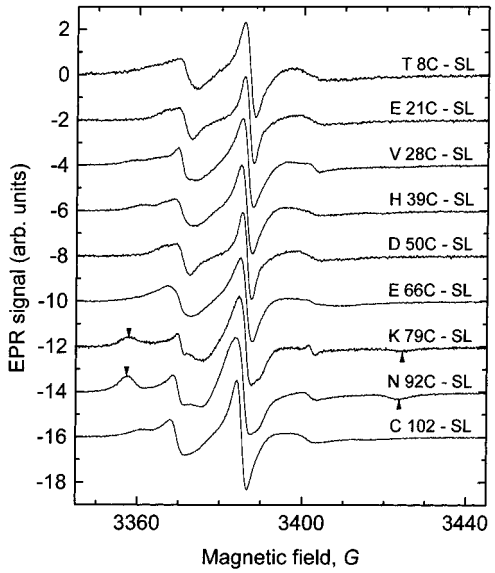

FIGURE 2: Comparison of the EPR spectra of labeled mutants in 30% sucrose, pH 5.0, and 0.05 M sodium acetate buffer. Gain = $\sim 3 \times 10^4$ with the signal normalized to the height of the central peak; modulation = 1.1 G; time constant = 50 ms; power = 0.2 mW. Each spectrum was the result of several 50 s accumulations. Apparatus: Murata-Erie-based DR, $\nu_e = 9.72$ GHz, sample size $\sim$ 1 μL, sample concentration $\sim$ 200 μM. Features marked by arrows are evidence of probe immobilization.

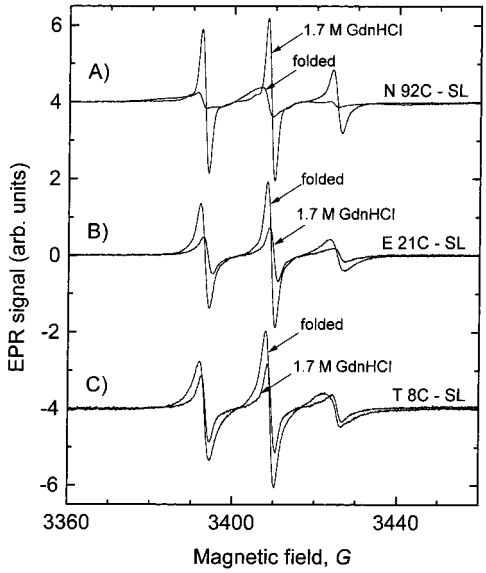

FIGURE 3: Spectra A present a comparison of the EPR spectrum at room temperature from N92C-SL as folded in pH 5.0, 0.05 M sodium acetate buffer with the corresponding GdnHCl-denatured spectrum in pH 5.0, 1.7 M GdnHCl. Spectra B and C provide the corresponding comparison of the EPR spectra from E21C-SL and T8C-SL, respectively, where the signal from the folded form is the more intense. These spectra were taken under room temperature EPR conditions as in Figure 2, except microwave power = 2 mW and modulation = 1.6 G. The sample concentrations and gains for each respective sample under folded and unfolded conditions were the same. The spectra of the GdnHCl-containing denatured protein slightly shift to higher field because the presence of GdnHCl slightly shifts the microwave resonant frequency of the sample.

unfolding was observed both by CD and by EPR peak height ratios (*12*) at 1.7 M GdnHCl, and less than 10% unfolding was observed at 0.85 M GdnHCl. Accordingly, kinetic refolding studies were performed by starting with protein unfolded in 1.7 M GdnHCl and mixing with buffer to a final GdnHCl concentration of 0.85 M.

EPR Characterization. The EPR spectra of spin-labeled mutant forms were measured in 30% sucrose to obtain spectral signatures of local probe motion indicating the degree of immobilization and localization of the probe (*8*), and we provide in Figure 2 a comparison of these spectra. According to methods of Mchaourab et al. (*8*), the purpose of the 30% sucrose is to remove the overall protein tumbling background while not quenching the local motion of the spin label. The majority of our labels in loop and external hydrophilic helical regions showed a narrow line width, less than 60 G splitting of outlying features, and overall evidence of the high mobility that had been observed from labels in comparable loop and external helical regions of T4 lysozyme. Although N92C-SL was externally located on the C helix and K79C-SL was externally located on the D loop, they both showed distinct outlying spin label features (arrows in Figure 2) with >60 G splittings which are evidence for immobilization of the probe on the protein. The splitting between the outlying arrowed high- and low-field features of N92C-SL (Figure 2), which is 66 $\pm$ 1 G, corresponds to a tumbling correlation time of 11 $\pm$ 3 ns.[2,3] This tumbling time is comparable with the calculated 10.4 ns tumbling time[2] of the entire cytochrome molecule in 30% sucrose.

In preparation for doing kinetics, comparisons of EPR signals were made between folded and GdnHCl-unfolded spin-labeled protein in dilute, nonviscous buffer. The reader should recognize that the kinetic changes which we measure at a single field on a particular sample represent the difference in the absorption first derivative ($d\chi''/dH$) EPR signal between folded and unfolded protein. The size of this difference between folded and unfolded signals will vary from one labeling site to another. For the majority of samples, such as N92C-SL, the derivative EPR line shape for unfolded protein is sharper and more intense because it reflects a less impeded subnanosecond correlation time, whereas the signal from folded protein is less intense because the label is impeded in its motion to the extent that its signal reflects correlation times approaching those of the protein itself ($\sim$3 ns). [For example, such correlation times have been estimated for C102-SL (*12*) from the peak height ratio of the three ^{14}N hyperfine features (*3*, *51*, *52*).] In Figure 3A we show EPR spectra of N92C-SL taken first under folded conditions and then under denatured conditions in GdnHCl; the latter denatured EPR derivative spectra are the more intense, as we routinely find. The two mutants E21C-SL and T8C-SL (Figure 3B,C) presented an unexpected contrast because there was a larger signal amplitude from their folded forms than

[2] $\tau_R = (4\pi r^3\eta)/(3kT)$, where η = solvent viscosity and r = Stokes radius of the rotating molecule (*55*). For iso-1-cyt *c*, $r \sim 15$ Å and $\eta = 0.03$ P in 30% sucrose at room temperature (*56*); τ_R is predicted to be 10.4 ns.

[3] For slow tumbling the empirical relation (*57*) was used: τ[ns] = $a(1 - S)^b$, where S is the ratio of the splitting between the experimental high-field and low-field derivative extremal features (arrows in Figure 2) to twice the A_z component of ^{14}N hyperfine coupling where $2A_z$ = 74 G (*58*). a and b are empirical constants depending on the intrinsic EPR line width. For an intrinsic line width of 3 G and Brownian rotation, $a = 0.54$ ns and $b = -1.36$. Thus, the splitting between the outlying arrowed high- and low-field features of N92C-SL (Figure 2), which is 66 $\pm$ 1 G, corresponds to a tumbling correlation time of 11 $\pm$ 3 ns.

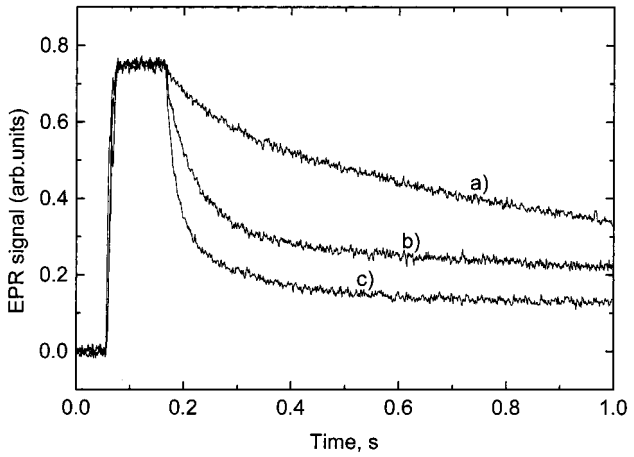

FIGURE 4: Comparison of the folding behavior of N92C-SL as shown on a 1 s time scale under conditions which lead to slow refolding (trace a) and faster folding (traces b and c). For trace a, initially unfolded protein in pH 5.0, 1.7 M GdnHCl was mixed in a 1:1 fashion with 0.05 M acetate buffer at pH 5.0 to initiate folding at a final GdnHCl concentration of 0.85 M. For trace b, initially unfolded protein at pH 2.0, 1.7 M GdnHCl was mixed in a 1:1 fashion with 0.05 M acetate buffer at pH 6.0 to initiate folding at a final GdnHCl concentration of 0.85 M and pH 5.0. For trace c, initially unfolded protein in pH 5.0, 1.7 M GdnHCl and 200 mM imidazole was mixed in a 1:1 fashion with 0.05 M acetate buffer and 200 mM imidazole at pH 5.0 to initiate folding at a final GdnHCl concentration of 0.85 M. EPR conditions were as follows: gain = $\sim 3 \times 10^4$; modulation = 1.7 G; time constant = 1 ms; power = 2 mW. Each trace required approximately 50 shots of 20 μL/shot.

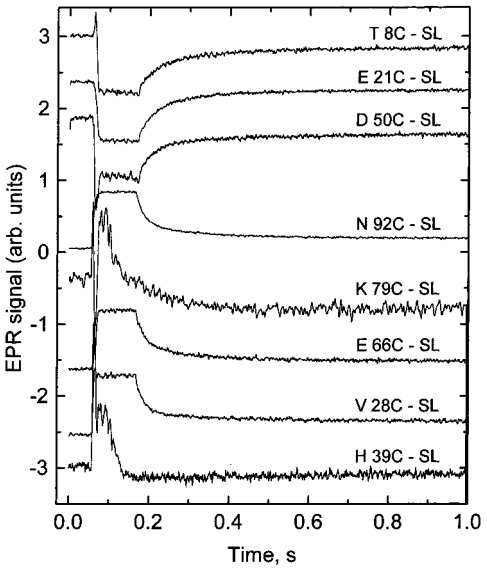

FIGURE 5: Refolding behavior as followed by stopped-flow EPR over a 1 s range under the imidazole conditions which led to fast folding in the 20−30 ms range for T8C-SL, E21C-SL, D50C-SL, N92C-SL, K79C-SL, E66C-SL, V28C-SL, and H39C-SL. Initially unfolded protein in pH 5.0, 1.7 M GdnHCl and 200 mM imidazole was mixed in a 1:1 fashion with 0.05 M acetate buffer and 200 mM imidazole at pH 5.0 to initiate folding at a final GdnHCl concentration of 0.85 M. EPR conditions were as follows: gain = $\sim 3 \times 10^4$; modulation = 1.7 G; time constant = 1 ms; power = 2 mW. K79C-SL and H39C-SL required 100 shots at 10 μL/shot so that the time for flow during a shot was half as long and the flow stopped sooner for these two samples. The other samples required approximately 50 shots at 20 μL/shot. The traces are shown normalized to approximately the same amplitude to make a convenient presentation. It should be noted that the overall amplitudes of the intrinsic recovery signal will vary from one site to the next because the signal difference between folded and unfolded protein will vary from one labeling site to the next. The traces which show the most noise are actually the ones from sites where the difference between folded and unfolded EPR signals was the smallest.

from their GdnHCl-unfolded forms, and we address its possible causes in the Discussion. At present we primarily use the kinetic variation of the difference between folded and unfolded signals as a kinetic probe, and the sign of the kinetic trace from T8C-SL and E21C-SL will be opposite to that of other mutants because their folded signal is greater than their unfolded signal.

Kinetic Results. Kinetic studies were generally carried out with the magnetic field on the peak of the central derivative EPR feature because EPR signal intensities were largest there, but for a given sample similar kinetics could be obtained from the other derivative features. Our kinetic work on iso-1-cyt *c* at its naturally occurring C102-SL had been carried out at pH 5.0, where we rapidly changed the GdnHCl concentration to induce folding (*12*, *13*). For times longer than a millisecond, such conditions had led to a transient signal from C102-SL which at 20 °C had a decay time in the 6 ms range attributed to fast folding in the C-terminal helical region (*13*). For all of our spin-labeled mutant samples (Table 1) the stopped-flow EPR study at pH 5 (in the absence of procedures to reduce potential heme misligation) showed a folding phase like that shown in Figure 4a for N92C-SL which occurred mostly with a decay time of about 1 s. A 1 s refolding time scale is 2 orders of magnitude longer than expected for the critical process of cytochrome folding associated with the formation of the N- and C-terminal helices (*18*−*21*). Using procedures reported in the literature to eliminate misligation, we folded N92C-SL in the presence of a high concentration of imidazole (*15*, *20*) or we used protein unfolded in GdnHCl at low pH (*53*) and initiated folding by mixing with high pH buffer to restore the pH to 5.0. As shown for N92C-SL, the former procedure (Figure 4c) with 200 mM imidazole provided a 20 ms refolding phase while the latter pH-dependent procedure (Figure 4b) provided a 50 ms phase. The kinetic traces indicating the 20−30 ms phases are shown for all mutant samples folded in the presence of 200 mM imidazole in the compendia of traces in Figure 5 taken over a time of 1 s. All samples had a minor phase with a decay time in the 15−25 s range which we show for N92C-SL in Figure 6. (In the Supporting Information we provide a comparison, Figure S-5A versus Figure S-5B, taken over a time of 10 s to show the slower folding for all mutants in the absence of imidazole versus the faster folding in the presence of imidazole.) Table 2 provides the phases and decay constants of folding processes in the presence of imidazole. (The corresponding times and phases in the absence of imidazole are give in Table S-5 of the Supporting Information.) The 20−30 ms recovery phase (phase A_1, τ_1, Table 2) occurred not only at T8C-SL and N92C-SL, which are in the N- and C-terminal helices, but with the possible exception of K79C-SL for which the overwhelming majority of signal change is over during the burst, all mutants showed this phase in the 20−30 ms regime, regardless of their location. There was a phase of lesser amplitude (A_2, τ_2, Table 2) in the 150 ms time scale. The majority of labels reported the minor 15−25 s phase (A_3, τ_3,

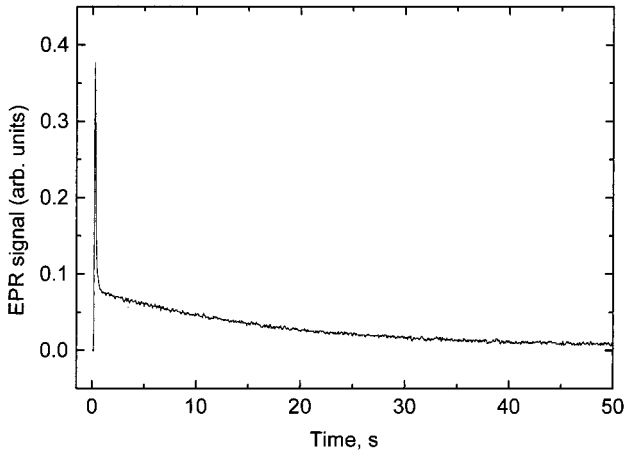

FIGURE 6: Slow refolding behavior as followed by stopped-flow EPR over a time of 50 s for the sample N92C-SL. Initially unfolded protein in pH 5.0, 1.7 M GdnHCl and 200 mM imidazole was mixed in a 1:1 fashion with 0.05 M acetate buffer and 200 mM imidazole at pH 5.0 to initiate folding at a final GdnHCl concentration of 0.85 M. EPR conditions were as follows: gain = $\sim 5 \times 10^3$; modulation = 1.7 G; time constant = 10 ms; power = 2 mW. The trace represents two accumulations.

Table 2). Except for N92C-SL,T8C-SL, and E21C-SL of the N- and C-terminal region, the remainder of the mutants both in the presence of imidazole and in its absence gave evidence of a sizable burst phase (A_0, Table 2) which occurred within the several millisecond dead time of the stopped-flow device. The burst is not directly visible in the transient stopped-flow mode with a mixer whose dead time is greater than several milliseconds; rather it is inferred from a difference in the signal between the completely unfolded protein signal and the signal during flow. An interesting detail of the folding of D50C-SL in the presence of imidazole was that the sign of the $\sim$20 ms and subsequent phases after the burst was reversed from that expected (i.e., the signal of D50C-SL increased in Figure 5).

Both in the presence and in the absence of imidazole, the mutants showing a burst phase are located toward the middle of the protein sequence. Although it is not the intent of this paper to characterize in great detail the time behavior of the burst, we did focus on D50C-SL, which had a particularly large burst phase signal, and we compared its burst phase to the previously measured burst from C102-SL. Using a rapid 65 μs minimal dead time ball mixer and flow EPR, we put limits on the time dependence of the very rapidly decreasing signal from D50C-SL at 5 °C (Figure 7) and compared it to the previously reported (*13*) submillisecond signals at room temperature and 7 °C from C102-SL. For D50C-SL there is extremely rapid probe immobilization occurring by the first time point at 65 μs so that we can say that the immobilization occurred on the 50 μs time scale even at 5 °C.

DISCUSSION

Characterization of Mutant Protein. The mass spectroscopic information directly indicated the purity of the protein. Unlike cysteine labeling of the naturally occurring Cys102, the cysteine-directed spin labeling at the external amino acid locations in Table 1 caused little perturbation to the far-UV CD helical signature (Figure S-3) or to the melting temperature and enthalpy of folding (Table S-3). For C102-SL, the MTSSL labeling had destabilized the wild-type cysteine site (*12*), whereas with our present externally located mutants, the MTSSL labeling left unperturbed or even slightly restabilized the cysteine mutant.

EPR Spectroscopic Information. The EPR signal of folded protein in 30% sucrose is an indicator of residual probe motion, and the overall line shape and central feature line width have been correlated with probe location by the systematic study of cysteine-directed spin labels in T4 lysozyme (*8*, *9*), and as explicitly determined from X-ray study of spin-labeled T4 lysozyme, solvent-exposed labels on a helix may experience immobilizing interaction with nearby residues, notably the fourth residue removed from the labeling site, and the nitroxide ring itself may be fixed by tertiary interaction with nearby side chains (*10*). As a broad general statement, helical and loop locations which have high solvent accessibility provide labeling sites with high mobility, and as indicated in Table S-4, Supporting Information, the iso-1-cyt *c* positions with high solvent accessibility (E21, T8C, D50, V28) have high mobility. The evidence from outlying EPR features of N92C-SL was that the spin label on N92C, where N92 does not have high solvent accessibility, was thoroughly immobilized with respect to the protein.[2,3] The additional implication was that there are no aggregates larger than a single cytochrome molecule which contribute to the EPR line shape of N92C-SL within folded iso-1-cyt *c*. K79C-SL also gave EPR evidence for a large probe immobilization. Examination of the iso-1-cyt c crystal structure (*37*) indicates closeness (<3.2 Å proximity) and tertiary interaction of the N92 side chain, which we replaced by spin-labeled C, to the sequentially distant Phe(−3) ring and of the K79 side chain, which we replaced by spin-labeled C, to sequentially distant Ser47. The implication is that tertiary interaction of sequentially distant regions may aid in the immobilization of the spin label.

The majority of our spin labels show a signal that is narrower and sharper when denatured by GdnHCl because the probe becomes more mobile when attached to denatured protein. A simple explanation is that the unfolded protein provides less defined structure to impede local probe motion. The comparison of folded and unfolded N92C-SL shows the expected behavior where the label signal is broad and less intense from the folded protein and narrower and sharper from the folded protein. Contrasting behavior occurred for E21C-SL and T8C-SL whose EPR signals were smaller from protein in denatured form. The positions of the label attachment for E21C-SL and T8C-SL happen to be close in sequence to the position of the paramagnetic heme, which is coupled to the protein at Cys14, Cys17, and His18. Thus, for E21C-SL and T8C-SL it is possible that remaining native structure near the heme may more severely restrict tumbling of a nearby spin label under unfolded conditions than when the label is on the exterior of the protein under folded conditions. Ratios of derivative peak heights (*3*, *51*, *52*) failed to indicate that the spin label was more mobile in the folded forms of E21C-SL or T8C-SL than in the GdnHCl-denatured forms of E21C-SL or T8C-SL. It is also possible that the spin label of E21C-SL or T8C-SL can more closely approach the heme in unfolded protein and experience greater dipolar broadening from the paramagnetic heme.[4]

Table 2: Observed Times and Percentage Amplitudes of Folding Phases for Spin-Labeled Iso-1-cyt *c*,[a] pH 5.0, plus 200 mM Imidazole

sample	A_0 (τ < 5 ms), %	A_1, %	τ_1, ms	A_2, %	τ_2, ms	A_3, %	τ_{3i}, s
T8C-SL	0	50 ± 1.7	33.8 ± 2.2	32 ± 1.8	168 ± 8	17.8 ± 1	14 ± 0.3
E21C-SL	0	57 ± 2.8	33.1 ± 1.5	31.3 ± 1.5	139 ± 6	13.5 ± 0.6	17.5 ± 0.8
V28C-SL	26 ± 2	48.9 ± 2.2	19.4 ± 0.4	9.6 ± 0.4	230 ± 2	15.4 ± 0.9	20.5 ± 0.8
H39C-SL	79 ± 4	21.4 ± 1	16.7 ± 0.4	0		−3.5 ± 0.2[b]	1.5 ± 0.2
D50C-SL	100	−55.5 ± 2.8[b]	29.5 ± 2.5	−18.9 ± 0.9[b]	234 ± 20	−15.2 ± 0.8[b]	13.7 ± 0.7
E66C-SL	33 ± 3	42 ± 4	21.5 ± 0.5	15.3 ± 0.1	149 ± 7	9.7 ± 0.6	23.4 ± 0.8
K79C-SL	84 ± 8	ND		15.6 ± 1	94 ± 3.5	−9.4 ± 0.4[b]	2.8 ± 0.2
N92C-SL	3 ± 2	58 ± 4.7	19.2 ± 0.5	24 ± 2.3	140 ± 15	17.6 ± 0.2	16.6 ± 0.2

[a] Time constants and percentage amplitudes of three kinetic phases plus the burst phase from EPR-detected folding experiments at 21 ± 1 °C. Refolding conditions were pH 5.0, 0.85 M GdnHCl, 0.05 M sodium acetate, and 200 mM imidazole. Signal percentages were calculated with respect to the difference between folded and unfolded EPR signals at equilibrium. [b] The negative sign indicates reversal of phase from the sign of the difference between folded and unfolded EPR signals at equilibrium.

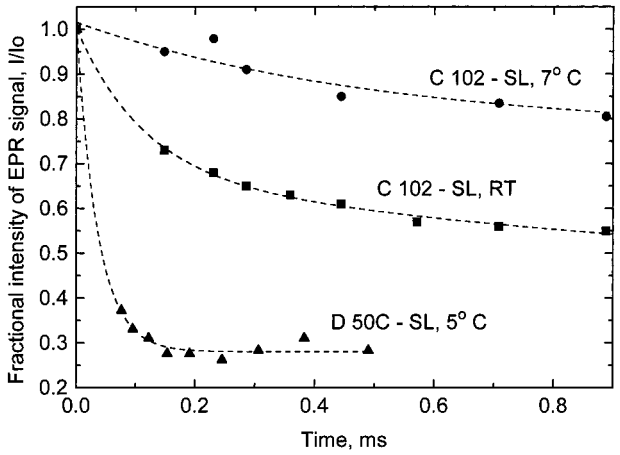

FIGURE 7: Comparison of the ultrarapid submillisecond folding/compacting as measured by rapid flow EPR (*13*) of D50C-SL at 5 °C with that of C102-SL at room temperature and 7 °C. For the D50C-SL sample 400 μM spin-labeled protein in 1.7 M GdnHCl was mixed 1:1 with dilute 0.1 M sodium acetate to obtain a 0.85 M GdnHCl concentration in which the protein was approximately 90% refolded, and for the C102-SL sample refolding was initiated by mixing unfolded protein in 0.8 M GdnHCl, pH 5.0, with pH 5.0, 0.05 M sodium acetate buffer to obtain a 0.4 M GdnHCl concentration in which the protein was ~70% refolded. The decrease of the fractional signal intensity I/I_0 from the central EPR feature of folding protein is shown as a function of the calibrated delivering time between the mixer and the center of the DR observation EPR zone. The decay time for folding/compaction of D50C-SL was estimated at 40 μs. Details of the corresponding longer times for C102-SL (a resolved 37% burst signal with an exponential time constant of 120 μs at 20 °C and a resolved 25% burst change with an exponential time constant of 500 μs at 7 °C) are provided in Grigoryants et al. (*13*).

Kinetics. The major goal of this work was to probe kinetics at numerous specific labeling sites throughout a folding protein. The methods reported previously that remove the kinetic trap of heme misligation either by added imidazole (*15*, *20*) or by folding from low pH (*53*) clearly worked to remove the 1 s folding phase. The work in these foregoing references was carried out on horse cytochrome (*15*, *20*, *53*). Although it may be that horse and yeast cytochromes fold by slightly different mechanisms, there is no doubt that the 1 s phase that disappears in the presence of imidazole or folding from low pH is heme misligation in both proteins. Thus we were able to perform a detailed comparison, as shown in Figure 5, of the folding of all of our mutants in the presence of imidazole which eliminated the apparent misligation step. A large percentage change attributed to the 20−30 ms phase did occur for T8C-SL and N92C-SL which are respectively on the hydrophilic sides of the N-terminal and C-terminal helices. These are the N- and C-helical regions which hydrogen exchange measurements would have identified as the location of early helix formation (*18*, *20*, *21*). However, all regions of the protein experienced the phase with 20−30 ms recovery time. The interesting reversal of sign for the 20−30 ms phase of D50C-SL may indicate a decreased probe immobilization and plausibly a local unfolding following the compaction of the burst. As reported by spin labels, the important 20−30 ms folding phase is more global in its nature than just the N- and C-terminal locale. There was no obvious evidence for a sequence of folding in the order of partially unfolded forms (PUFS) I, II, III, IV (Table 1) as had been predicted from native state hydrogen exchange (*21*, *22*). *The global nature of the 20−30 ms phase, which our site-directed spin labels report, is a simple yet important finding for the folding of cytochrome c.* A major criticism of spin labels has been that they perturb the phenomena they measure; the general evidence of our study is that our spin labels are reporting common themes and not highly perturbed, disconnected kinetic events.

There were also minority phases with longer decay times observed. The phase with decay time in the 15−25 s regime (Figure 6) is most likely due to recovery from cis/trans isomerization of prolyl peptide bonds (*26*). There is also a minority phase with decay time of ~150 ms, and we do not know the cause of this phase.

The ultrafast component reported by flow EPR from D50C-SL showed probe immobilization on the 50 μs time scale even at 5 °C, which was an order of magnitude faster immobilization than C102-SL showed (~500 μs at 7 °C) at a comparable temperature (*13*). It is possible that D50 lies in or near an initiation site where a loop rapidly forms on the 50 μs time scale (*54*); the region where D50 is located is not one where early helical structure occurs (*18*), nor is it in a hydrophobic region, as is the cysteine sulfur of C102. C102-SL, whose cysteine attachment site originated in the hydrophobic core of the C terminus, definitely did report a burst (*13*), but we find that T8C-SL, E21C-SL, and N92C-SL, whose spin labels are respectively attached to the

[4] The dipolar broadening effect is subtle because, as Leigh showed (*59*), the dipolar interaction with a protein-bound paramagnetic metal will broaden a nearby spin label signal at most orientations of the spin label except those orientations near the magic angle defined by the metal-to-nitroxide vector and the direction of the applied magnetic field. For these orientations the line remains narrow, albeit diminished in intensity.

hydrophilic regions of the N- and C-terminal helices, do not show the burst. Other sites (V28, H39, E66, and K79 as well as D50) exist where stopped-flow EPR indicates a substantial percentage of burst. It would appear that the external labels in regions away from the ends of the sequence are ones enfolded in the initial submillisecond folding or prefolding event.

ACKNOWLEDGMENT

The authors thank Prof. B. Bowler and Prof. G. Pielak for providing pBTR1 plasmids containing the yeast iso-1-cyt *c* gene and the heme lyase gene. We gratefully acknowledge the aid given to us by Dr. C. Hauer, Wadsworth Center for Laboratories and Research, Albany, NY, in obtaining mass spectroscopic information on the molecular weights of our iso-1-cyt *c* mutants.

SUPPORTING INFORMATION AVAILABLE

Text, Figures S-1 and S-2, and Table S-1 explaining in detail the method of megaprimer mutagenesis for making cysteine-directed mutants of iso-1-cyt-c, for expressing the iso-1-cyt *c* in *E. coli*, for purifying the recombinant protein, and for spin labeling the protein; Table S-2 providing a summary of molecular weights of mutant proteins determined by mass spectroscopy; Table S-3 presenting thermodynamic folding parameters for all mutants; Table S-4 listing the mobility of cysteine-directed spin labels and correlation with solvent accessibility; Table S-5 listing times and percentage amplitudes of refolding phases in the absence of imidazole; Figure S-3 presenting a comparison of CD-monitored thermal denaturation of N92C, N92C-SL, and C102S; Figure S-4 presenting a CD-detected thermal melting curve for C102S, N92C, and N92C-SL; and Figures S-5A and S-5B respectively showing refolding kinetics over a 10 s time range in the absence and the presence of imidazole. This material is available free of charge via the Internet at http://pubs.acs.org.

REFERENCES

1. Berliner, L. J. (1978) *Spin Labeling: Theory and Applications*, Academic Press, New York.
2. Schneider, D. J., and Freed, J. H. (1989) in *Biological Magnetic Resonance* (Berliner, L., and Ruben, J., Eds.) pp 1−76, Chapter 1, Plenum, New York.
3. Marsh, D. (1989) in *Biological Magnetic Resonance* (Berliner, L., and Ruben, J., Eds.) pp 255−303, Chapter 5, Plenum, New York.
4. Hubbell, W. L., and Altenbach, C. (1994) *Curr. Opin. Struct. Biol. 4*, 566−573.
5. Hubbell, W. L., Gross, A., Langen, R., and Lietzow, M. A. (1998) *Curr. Opin. Struct. Biol. 8*, 649−656.
6. Hubbell, W. L., Mchaourab, H. S., Altenbach, C., and Lietzow, M. A. (1996) *Structure 4*, 779−783.
7. Hubbell, W. L., Cafiso, D. S., and Altenbach, C. (2000) *Nat. Struct. Biol. 7*, 735−739.
8. Mchaourab, H. S., Lietzow, M. A., Hideg, K., and Hubbell, W. L. (1996) *Biochemistry 35*, 7692−7704.
9. Mchaourab, H. S., Kalai, T., Hideg, K., and Hubbell, W. L. (1999) *Biochemistry 38*, 2947−2955.
10. Langen, R., Oh, K. J., Cascio, D., and Hubbell, W. L. (2000) *Biochemistry 39*, 8396−8405.
11. Sienkiewicz, A., Qu, K., and Scholes, C. P. (1994) *Rev. Sci. Instrum. 65*, 68−74.
12. Qu, K., Vaughn, J. L., Sienkiewicz, A., Scholes, C. P., and Fetrow, J. S. (1997) *Biochemistry 36*, 2884−2897.
13. Grigoryants, V. M., Veselov, A. V., and Scholes, C. P. (2000) *Biophys. J. 78*, 2702−2708.
14. Tsong, T. Y. (1976) *Biochemistry 15*, 5467−5473.
15. Brems, D. N., and Stellwagen, E. (1983) *J. Biol. Chem. 258*, 3655−3660.
16. Nall, B. T., and Landers, T. A. (1981) *Biochemistry 20*, 5403−5411.
17. Colón, W., Elöve, G. A., Wakem, L. P., Sherman, F., and Roder, H. (1996) *Biochemistry 35*, 5538−5549.
18. Roder, H., Elöve, G. A., and Englander, S. W. (1988) *Nature 335*, 700−704.
19. Elöve, G. A., Chaffotte, A. F., Roder, H., and Goldberg, M. E. (1992) *Biochemistry 31*, 6876−6883.
20. Elöve, G. A., Bhuyan, A. K., and Roder, H. (1994) *Biochemistry 33*, 6925−6935.
21. Englander, S. W., Sosnick, T. R., Mayne, L. C., Shtilerman, M., Qi, P. X., and Bai, Y. (1998) *Acc. Chem. Res. 31*, 737−744.
22. Bai, Y., Sosnick, T. R., Mayne, L., and Englander, S. W. (1995) *Science 269*, 192−197.
23. Bai, Y., and Englander, S. W. (1996) *Proteins 24*, 145−151.
24. Pierce, M. M., and Nall, B. T. (1997) *Protein Sci. 6*, 618−627.
25. Pierce, M. M., and Nall, B. T. (2000) *J. Mol. Biol. 298*, 955−969.
26. Osterhout, J. J., Jr., and Nall, B. T. (1985) *Biochemistry 24*, 7999−8005.
27. Creighton, T. E. (1994) *Nat. Struct. Biol. 1*, 135−138.
28. Sosnick, T. R., Shtilerman, M. D., Mayne, L., and Englander, S. W. (1997) *Proc. Natl. Acad. Sci. U.S.A. 94*, 8545−8550.
29. Winkler, J. R., and Gray, H. B. (1998) *Acc. Chem. Res. 31*, 698.
30. Shastry, M. C. R., Sauder, J. M., and Roder, H. (1998) *Acc. Chem. Res. 31*, 717−725.
31. Eaton, W. A., Munoz, V., Thompson, P. A., Henry, E. R., and Hofrichter, J. (1998) *Acc. Chem. Res. 31*, 745−753.
32. Yeh, S. R., and Rousseau, D. L. (1998) *Nat. Struct. Biol. 5*, 222−228.
33. Telford, J. R., Wittung-Stafshede, P., Gray, H. B., and Winkler, J. R. (1998) *Acc. Chem. Res. 31*, 755−763.
34. Pollack, L., Tate, M. W., Darnton, N. C., Knight, J. B., Gruner, S. M., Eaton, W. A., and Austin, R. H. (1999) *Proc. Natl. Acad. Sci. U.S.A. 96*, 10115−10117.
35. Shastry, M. C., and Roder, H. (1998) *Nat. Struct. Biol. 5*, 385−392.
36. Sienkiewicz, A., da Costa Ferreira, A. M., Danner, B., and Scholes, C. P. (1999) *J. Magn. Reson. 136*, 137−142.
37. Louie, G. V., and Brayer, G. D. (1990) *J. Mol. Biol. 214*, 527−555.
38. Moore, G. R., and Pettigrew, G. W. (1990) *Cytochromes c Evolutionary, Structural and Physicochemical Aspects*, Springer-Verlag, Berlin.
39. Pollock, W. B., Rosell, F. I., Twitchett, M. B., Dumont, M. E., and Mauk, A. G. (1998) *Biochemistry 37*, 6124−6131.
40. Morar, A. S., Kakouras, D., Young, G. B., Boyd, J., and Pielak, G. J. (1999) *J. Biol. Inorg. Chem. 4*, 220−222.
41. Bowler, B. E., May, K., Zaragoza, T., York, P., Dong, A., and Caughey, W. S. (1993) *Biochemistry 32*, 183−190.
42. Mayo, S. L., Ellis, W. R., Jr., Crutchley, R. J., and Gray, H. B. (1986) *Science 233*, 948−952.
43. Kammann, M., Laufs, J., Schell, J., and Gronenborn, B. (1989) *Nucleic Acids Res. 17*, 5404.
44. Landt, O., Grunert, H. P., and Hahn, U. (1990) *Gene 96*, 125−128.
45. Ke, S. H., and Madison, E. L. (1997) *Nucleic Acids Res. 25*, 3371−3372.
46. Sarkar, G., and Sommer, S. S. (1992) *Nucleic Acids Res. 20*, 4937−4938.
47. Murphy, M. E., Fetrow, J. S., Burton, R. E., and Brayer, G. D. (1993) *Protein Sci. 2*, 1429−1440.
48. Mulligan-Pullyblank, P., Spitzer, J. S., Gilden, B. M., and Fetrow, J. S. (1996) *J. Biol. Chem. 271*, 8633−8645.
49. Fetrow, J. S., Horner, S. R., Oehrl, W., Schaak, D. L., Boose, T. L., and Burton, R. E. (1997) *Protein Sci. 6*, 197−210.

50. Margoliash, E., and Frohwit, N. (1959) *Biochem. J. 71*, 570−572.
51. Todd, A. P., and Millhauser, G. L. (1991) *Biochemistry 30*, 5515−5523.
52. Bales, B. L. (1989) in *Biological Magnetic Resonance* (Berliner, L., and Ruben, J., Eds.) pp 77−130, Chapter 2, Plenum, New York.
53. Sosnick, T. R., Mayne, L., Hiller, R., and Englander, S. W. (1994) *Nat. Struct. Biol. 1*, 149−156.
54. Hagen, S. J., Hofrichter, J., Szabo, A., and Eaton, W. A. (1996) *Proc. Natl. Acad. Sci. U.S.A. 93*, 11615−11617.
55. Carrington, A., and McLachlan, D. M. (1969) *Introduction to Magnetic Resonance*, Harper and Row, New York, NY.
56. Mchaourab, H. S., Oh, K. J., Fang, C. J., and Hubbell, W. L. (1997) *Biochemistry 36*, 307−316.
57. Freed, J. H. (1976) in *Spin Labeling, Theory and Applications* (Berliner, L. J., Ed.) Acadmic Press, New York.
58. Columbus, L., Kalai, T., Jeko, J., Hideg, K., and Hubbell, W. L. (2001) *Biochemistry 40*, 3828−3846.
59. Leigh, J. S. (1970) *J. Chem. Phys. 52*, 2608−2612.

BI011414N